Structural and Functional Models of the Dimanganese Catalase Enzymes. 2. Structure, Electrochemical, Redox, and EPR Properties

P. J. Pessiki, S. V. Khangulov, D. M. Ho, and G. C. Dismukes*

Contribution from the Princeton University, Department of Chemistry, Henry H. Hoyt Laboratory, Princeton, New Jersey 08544

Received July 16, 1993®

Abstract: Catalysts which functionally mimic the bacterial dimanganese catalase enzymes have been synthesized and their structure, electrochemical, redox, and EPR spectra have been compared to the enzyme. These compounds are formulated as $[LMn_2^{II,II}X]Y_2$, μ-X = CH_3CO_2, $ClCH_2CO_2$; Y = ClO_4, BPh_4, CH_3CO_2, possessing a bridging μ-alkoxide from the ligand, HL = *N,N,N',N'*-tetrakis(2-methylenebenzimidazole)-1,3-diaminopropan-2-ol. An X-ray diffraction structure of $[LMn_2(CH_3CO_2)(butanol)](ClO_4)_2 \cdot H_2O$, in the monoclinic space group $P2(1)/c$, confirmed the anticipated N_6O septadentate coordination of the HL ligand, the bridging μ-acetate, and revealed both five- and six-coordinate Mn ions; the latter arising from a butanol solvent molecule. This contrasts with the six-coordinate Mn ions observed for the μ-Cl and μ-OH derivatives, LMn_2Cl_3 and $LMn_2(OH)Br_2$ (Mathur et al. *J. Am. Chem. Soc.* **1987**, *109*, 5227–5232). Like the enzyme, three electrons can be removed from these complexes to form four oxidation states ranging from $Mn_2^{II,II}$ to $Mn_2^{III,IV}$. Three of these have been characterized by EPR and found to possess electronic ground states, Mn^{III} electron orbital configurations, ^{55}Mn hyperfine parameters, and Heisenberg exchange interactions analogous to those observed in the enzyme. For the μ-carboxylate derivatives electrochemistry reveals the initial oxidation process involves loss of two electrons at 0.81–0.86 V, forming $Mn_2^{III,III}$, followed by dismutation to yield a $Mn_2^{II,III}$ and $Mn_2^{III,IV}$ species. By contrast, the μ-Cl and μ-OH derivatives oxidize by an initial one-electron process (0.49–0.54 V). For the μ-carboxylate derivatives chemical oxidation with $Pb(OAc)_4$ also reveals an initial two-electron oxidation to a $Mn_2^{III,III}$ species, which dismutates to form both $Mn_2^{II,III}$ and $Mn_2^{III,IV}$ species. The two $Mn_2^{II,III}$ species formed by these methods exhibit ^{55}Mn hyperfine fields differing in magnitude by 9% (150 G), implying different Mn coordination environments induced by the electrolyte. The different ligand coordination observed in the enzyme (predominantly oxo and carboxylato) appears to be responsible for stabilization of the $MnCat^{III,III}$ oxidation state as the resting state.

Introduction

Some bacterial catalases[1] found in thermophillic or lactate-rich sources possess a rare dimanganese active site, in contrast to the more widely distributed monoheme cofactor of iron catalases.[2] These function to catalyze the disproportionation of hydrogen peroxide, eq 1, created by all aerobic cells.

$$2H_2O_2 \rightarrow O_2 + 2H_2O \quad (1)$$

Catalysis appears to involve both Mn ions which are located within 3.6 Å to one another.[3] Four oxidation states of the enzyme have been identified. The *Thermus thermophilus* (*Tt*) enzyme exhibits characteristic EPR signals in three of these oxidation states, $Mn_2^{II,II}$, $Mn_2^{II,III}$, and $Mn_2^{III,IV}$. This has facilitated mechanistic studies of peroxide dismutation which support a "ping-pong" mechanism involving the $Mn_2^{II,II}/Mn_2^{III,III}$ oxidation states.[4] The same oxidation states are also favored for the enzyme isolated from *Lactobacillus plantarum*, based on XANES, EXAFS, and electronic absorption spectroscopies.[5] The evidence which directly implicates the $Mn_2^{III,III}$ oxidation state in catalase activity is uncertain. Optical and EPR spectral data from functional catalase mimics would aid interpretation of the available enzyme data, but so far have been reported only for the $Mn_2^{II,II}$ oxidation state.[6a] A preliminary account of the present work has appeared.[6b]

Although there has been much progress in synthetic modeling of multinuclear manganese enzymes,[7] functionally active synthetic analogs have received little attention. Manganese dimers and trimers have been reported which exhibit catalase activity involving manganese dissociation/reassociation which is not observed for

† Keywords: manganese, catalase, hydrogen peroxide, enzyme, electrochemical, EPR, X-ray synthesis.

® Abstract published in *Advance ACS Abstracts*, January 1, 1994.

(1) (a) Kono, Y.; Fridovich, I. *J. Biol. Chem.* **1983**, *258*, 6015–6019. (b) Kono, Y.; Fridovich, I. *J. Biol. Chem.* **1983**, *258*, 13646–13648. (c) Vainshtein, B. K.; Melik-Adamyan, V. R.; Barynin, V. V.; Vagin, A. A. *Progress in Bioorganic Chemistry and Molecular Biology*; Ovchinnikov, Yu, Ed.; Elsevier. Publ.: Amsterdam, 1984; pp 117–132. (d) Barynin, V. V.; Grebenko, A. I. *Doklady Acad. Sci., USSR* **1986**, *286*, 461–464. (e) Allgood, G. S.; Perry, J. J. *J. Bacteriol.* **1986**, *168*, 563–567.

(2) Schonbaum, G. R.; Chance, B. In *The Enzymes*, 3rd ed.; Boyer, P., Ed.; Academic Press: New York, 1978; Vol. 13, p 363.

(3) (a) Vainshtein, B. K.; Melik-Adamyan, W. R.; Barynin, V. V.; Vagin, A. A.; Grebenko, A. I. *Proc. Int. Symp. Biomol. Struct. Interactions Suppl J. Biosci.* (*1&2*), **1985**, *8*, 471–479. (b) Barynin, V. V.; Vagin, A. A.; Melik-Adamyan, W. R.; Grebenko, A. I.; Khangulov, S. V.; Popov, A. N.; Andrianova, M. E.; Vainshtein, B. K. *Dokl. Akad. Nauk. SSSR* [*Crystallogr.*] **1986**, *288* (4), 877–880 (Russ).

(4) (a) Khangulov, S. V.; Barynin, V. V.; Melik-Adamyan, V. R.; Grebenko, A. I.; Voevodskay, N. V.; Blumenfeld, L. A.; Dobrykov, S. N.; Il'ysova, V. B. *Bioorgan. Khimiya* **1986**, *12*, 741–748 (Russ.). (b) Khangulov, S. V.; Voyevodskaya, N. V.; Barynin, V. V.; Grebenko, A. I.; Melik-damyan, V. R. *Biofizika* **1987**, *32*, 1044–1051 (Engl.), 960–966 (Russ.). (c) Khangulov, S. V.; Barynin, V. V.; Antonyuk-Barynina, S. V. *Biochim. Biophys. Acta* **1990**, *1020*, 25–33. (d) Khangulov, S. V.; Barynin, V. V.; Voevodskaya, N. V.; Grebenko, A. I.; *Biochim. Biophys. Acta* **1990**, *1020*, 305–310. (e) Khangulov, S. V.; Andreeva, N. E.; Gerasimenko, V. V.; Goldfeld, M. G.; Barynin, V. V.; Grebenko, A. I. *Russ. J. Phys. Chem.* **1990**, *64*, 10–16. (f) Khangulov, S. V.; Goldfeld, M. G.; Gerasimenko, V. V.; Andreeva, N. E.; Barynin, V. V.; Grebenko, A. I. *J. Inorg. Biochem.* **1990**, *40*, 279–292.

(5) (a) Penner-Hahn, J. E. In *Manganese Redox Enzymes*; Pecoraro, V. L., Ed.; Verlag Chemie: New York, 1992; pp 29–46. (b) Waldo, G. S.; Fronko, R. M.; Penner-Hahn, J. E. *Biochemistry* **1991**, *30*, 10486–10490. (c) Waldo, G. S.; Yu, S.; Penner-Hahn, J. E. *J. Am. Chem. Soc.* **1992**, *114*, 5869–5870. (d) Vanngard, T.; Hansson, O.; Haddy, A. In *Manganese Redox Enzymes*; Pecoraro, V. L., Ed.; Verlag Chemie: New York, 1992; pp 105–118.

(6) (a) Mathur, P.; Crowder, M.; Dismukes, G. C. *J. Am. Chem. Soc.* **1987**, *109*, 5227–5232. (b) Pessiki, P. J.; Khangulov, S. V.; Dismukes, G. C.; Barynin, V. V. In *Macromolecular Host-Guest Complexes: Optical, Optoelectronic and Photorefractive Properties and Applications*; Jenheke, S., Ed.; Materials Research Society: Pittsburgh, PA 1992; Vol. 277, pp 75–86.

(7) (a) Christou, G. *Acc. Chem. Res.* **1989**, *22*, 328–335. (b) Wieghardt, K. *Angew. Chem., Int. Ed. Engl.* **1989**, *28*, 1153–1172. (c) Pecoraro, V. L. *Photochem. Photobiol.* **1988**, *48*, 249–264.

0002-7863/94/1516-0891$04.50/0

the enzyme.[8] This has motivated us to extend our original studies of a functional catalase mimic[6] to synthesize new derivatives which would be amenable to structural characterization and which access all four oxidation states known to form in the enzyme.

These new derivatives, noted below, differ from our previous catalase mimics by replacing μ-bridging and terminal anions, Cl^- or OH^- and Br^-, by a bridging μ-carboxylate and noncoordinating ClO_4^- or BPh_4^- counterions. We report the first X-ray diffraction structure of a member of this series, $[LMn_2(CH_3CO_2)][(ClO_4)_2 \cdot H_2O$. The replacement of μ-Cl or μ-OH by μ-carboxylate changes significantly the electrochemical and redox properties of these compounds. Here we also provide the first spectroscopic evidence for formation of both the $Mn_2^{II,III}$ and $Mn_2^{III,IV}$ oxidation states in these compounds and compare their EPR spectra to the corresponding enzyme spectra.

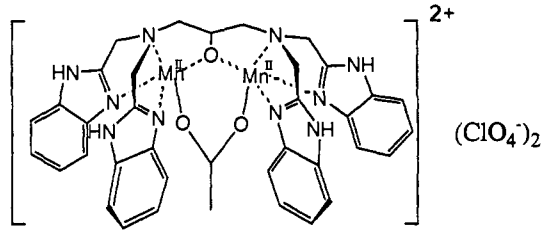

LMn_2XY_2; X = CH_3CO_2, $ClCH_2CO_2$; Y = CH_3CO_2, ClO_4, BPh_4

Experimental Section

$[LMn_2(CH_3CO_2)](ClO_4)_2$. The ligand was synthesized as previously described.[6] The ligand, *N,N,N',N'*-tetrakis(2-methylenebenzimidazolyl)-1,3-diaminopropan-2-ol (HL) (366 mg, 0.6 mmol), 60 mg (1 mmol) of acetic acid, and 272 mg of (2 mmol) $NaOAc \cdot 3H_2O$ were combined in 100 mL of a premixed 3:1 ethanol–water solution. After stirring for 15 min, 245 mg (1.0 mmol) of $Mn^{II}(OAc)_2 \cdot 4H_2O$ dissolved in 15 mL of ethanol was added. The mixture was allowed to stir for 30 min, after which time 1.12 g (8 mmol) of $NaClO_4 \cdot H_2O$ was added as an ethanolic water solution. The reaction mixture was allowed to stir for 1 h, and then the volume was reduced under vacuum. Upon standing a crystalline precipitate formed (330 mg, 61%) which was collected by filtration.

Spectral data for $[LMn_2(CH_3CO_2)](ClO_4)_2$: FT-IR (KBr, cm^{-1}), μ_2-carboxylate 1564 (unsymmetrical) and 1428 (symmetrical); FAB mass spectrometry (% int.) corresponding to the monocation $\{[LMn_2(CH_3CO_2)](ClO_4)\}^{1+}$ MW 877 (69.6%). Anal. Calcd (found) $LMn_2(CH_3CO_2)(ClO_4)_2$: C, 45.3 (45.4); H, 3.79 (3.69); N, 14.2 (14.3); Cl, 6.9 (7.2).

The product was recrystallized from $CH_2Cl_2/CHCl_3$/butanol to yield crystals suitable for diffraction. Two other derivatives noted below were prepared in a similar manner.

$[LMn_2(CH_3CO_2)](BPh_4)_2$. Spectral data: FT-IR (KBr, cm^{-1}), μ_2-carboxylate 1564 (unsymmetrical) and 1427 (symmetrical); FAB mass spectrometry (% int.) corresponding to the monocation $\{[LMn_2(CH_3CO_2)](ClO_4)\}^{1+}$ MW 1097 (15%). Anal. Calcd (found) $LMn_2(CH_3CO_2^-)(BPh_4^-)_2$: C, 72.0 (70.7); H, 5.58 (5.4); N, 9.0 (10.3); B, 1.23 (1.5).

$[LMn_2(ClCH_2CO_2)](ClO_4)_2$. Spectral data: FT-IR (KBr, cm^{-1}), μ_2-carboxylate 1598 (unsymmetrical) and 1404 (symmetrical); FAB mass spectrometry (% int.) corresponding to the monocation $\{[LMn_2(ClCH_3CO_2)](ClO_4)\}^{1+}$ MW 911 (70.0%). Anal. Calcd (found) $LMn_2(ClCH_3CO_2)(ClO_4)_2$: C, 43.9 (43.9); H, 3.28 (3.46); N, 13.6 (13.8); Cl, 10.3 (10.5).

Instrumentation. Electrochemistry. Cyclic voltammetry was performed with a Model 363 potentiostat in line with a Model 175 Universal Programmer (Princeton Applied Research). In all experiments a three electrode system was used: Pt|Pt|SCE. Measurements were performed in acetonitrile using tetra-*n*-butylammonium perchlorate as the supporting electrolyte, concentration 1×10^{-3} M manganese complex at scan rate 100 mv/s. All solutions were degassed prior to the experiments.

EPR spectra at 9.34 GHz were obtained with a Bruker ESP-300 spectrometer in the temperature range 4.2–77 K using an Oxford Instruments ESR-900 continuous flow cryostat. In experiments where there were mixtures of more than one oxidation state, it was possible to detect the $Mn_2^{II,III}$ EPR signal in the presence of the $Mn_2^{III,IV}$ species because of large differences in their temperature dependencies and spin relaxation rates. At low temperature (10 K) and high power only the $Mn_2^{II,III}$ state can be detected. When the temperature is raised to 60 K, the $Mn_2^{II,III}$ state undergoes efficient relaxation broadening, and only the $Mn_2^{III,IV}$ state can be detected.

IR and UV–vis Studies. Mid-IR samples (4000–600 cm^{-1}) were prepared using KBr (1%) and run on a Nicolet 730 FTIR. The far IR samples (600–125 cm^{-1}) were prepared using CsI (5%) and run on a Nicolet 800 FTIR collecting 125 scans on average. UV–vis spectrophotometry was recorded with a Hewlett-Packard HP-8450A.

Table 1. Summary of the Crystal Structure Data for $[LMn_2(CH_3CO_2)(butanol)](ClO_4)_2(H_2)$[a]

formula	$C_{41}H_{48}Cl_2Mn_2N_{10}O_{13}$
formula wt	1069.7
space group	monoclinic $P2(1)/c$
a, Å	16.664(2)
b, Å	11.652(2)
c, Å	24.687(3)
β, deg	97.24(1)
Z	4
V, Å^3	4756(1)
reflcns: unique/obsd ($F > 3\sigma$)	8413/4333
no. of params	591
S	1.31
$R(F)$	8.35%
$wR(F)$	8.41%

[a] $S = [\sum w(|F_o| - |F_c|)^2/(M-N)]^{1/2}$ where M is the number of observed reflections, and N is the number of parameters refined. $R(F) = \sum||F_o| - |F_c||/\sum|F_o|$. $wR(F) = [\sum w(|F_o| - |F_c|)^2/(\sum w(|F_o|^2)]^{1/2}$.

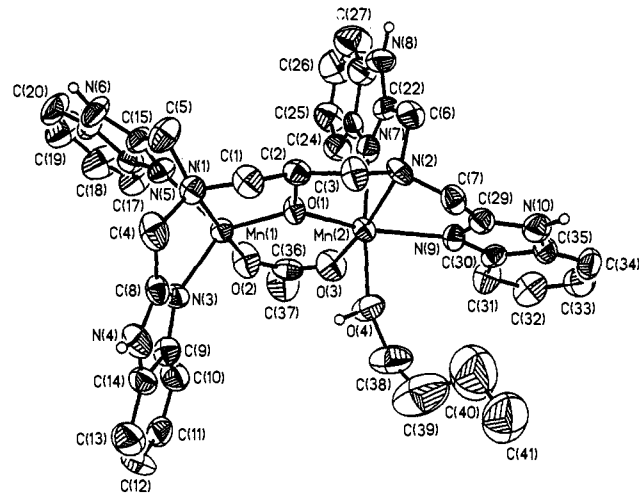

Figure 1. Crystal structure of the cation $[LMn_2(CH_3CO_2)]^{2+}$.

Results

Crystallography. A single crystal of $[LMn_2(CH_3CO_2)(butanol)](ClO_4)_2 \cdot H_2O$ with dimensions $0.18 \times 0.20 \times 0.30$ mm was mounted on a Siemens P4 four-circle diffractometer for data collection. The structure was solved by heavy-atom methods (XS:PATT) in the monoclinic space group $P2_1/c$ (no. 14) and defined by full-matrix least-squares.[9] Table 1 summarizes the crystallographic data. A full report of the refinement procedure and atomic coordinates is available as supplementary material.

The solid-state structure consists of discrete dimanganese^{II,III} complex cations, perchlorate anions, and waters of hydration. A view of the $[LMn_2(CH_3CO_2)(butanol)]^{2+}$ cation is shown in Figure 1, and selected distances and angles are listed in Table 2. The two Mn atoms within the complex exhibit different coor-

(8) (a) Rush, J. D.; Maskos, Z. *Inorg. Chem.* **1990**, *29*, 897–905. (b) Larson, E. J.; Pecoraro, V. L. *J. Am. Chem. Soc.* **1991**, *113*, 7809–7810.

(9) (a) Sheldrick, G. M. SHELXTL PLUS 4.21 for Siemens Crystallographic Research Systems: Siemens Analytical X-ray Instruments, Inc.: Madison WI, 1990. (b) All computations were performed on a MicroVAX computer. All non-hydrogen scattering factors were corrected for both real and imaginary components of anomalous dispersion.

Table 2. Selected Bond Lengths (Å) and Angles (deg) for $[LMn_2(OAc)(butanol)](ClO_4)_2(H_2O)$

Selected Bond Lengths (Å)			
Mn(1)–O(1)	2.015(5)	Mn(2)–O(1)	2.086(6)
Mn(1)–O(2)	2.052(7)	Mn(2)–O(3)	2.099(6)
Mn(1)–N(1)	2.475(7)	Mn(2)–N(2)	2.422(7)
Mn(1)–N(3)	2.129(8)	Mn(2)–N(7)	2.211(8)
Mn(1)–N(5)	2.158(8)	Mn(2)–N(9)	2.235(7)
Mn(1)–Mn(2)	3.540(2)	Mn(2)–O(4)	2.248(7)
Selected Bond Angles (deg)			
O(1)–Mn(1)–N(3)	115.9(3)	O(1)–Mn(2)–O(4)	85.8(3)
O(1)–Mn(1)–N(5)	121.9(3)	O(1)–Mn(2)–N(7)	91.8(3)
N(3)–Mn(1)–N(5)	103.6(3)	O(4)–Mn(2)–N(9)	83.8(3)
		N(7)–Mn(2)–N(9)	91.5(3)

dination numbers and geometries. Mn(1) is five-coordinate and has a N_3O_2 distorted trigonal-bipyramidal geometry. Mn(2) is six-coordinated and roughly octahedral with a N_3O_3 coordination sphere. Two benzimidazole moieties and a tertiary amine from one-half of the heptadentate ligand L are coordinated to Mn(1), while an analogous set of three nitrogens from the remaining half of the ligand are coordinated to Mn(2). The two Mn atoms are bridged by the L alkoxo functional group and also by a bidentate (syn–syn) acetate ligand. Lastly, the coordination sphere of Mn(2) is expanded to six-coordinate via the additional binding of a butanol solvent molecule.

The average Mn(1)–N(benzimidazole) and Mn(2)–N(benzimidazole) distances are 2.144 and 2.223 Å, while the Mn(1)–N(amine) and Mn(2)–N(amine) distances are significantly longer at 2.475 and 2.422 Å, respectively. The μ-alkoxo O(1) atom forms a symmetrical bridge between Mn(1) and Mn(2) with observed distances of 2.015 and 2.086 Å, respectively. The Mn(1)–O(2) and Mn(2)–O(3) distances to the bridging acetate are 2.052 and 2.099 Å, and are also normal. The Mn(1)···Mn(2) separation of 3.540 Å and Mn(1)–O(1)–Mn(2) angle of 119.4° are comparable to values observed in related dinuclear complexes bridged by one alkoxo and one carboxylate ligand.[10] The bonds to Mn(1) are slightly shorter than those to Mn(2) except for a reversal in the amine linkages where Mn(1)–N(1) > Mn(2)–N(2). All of these features are consistent with the lower coordination number and trigonal-bipyramidal geometry of the Mn(1) atom. Similar observations have been reported for a related dimanganese^{II,II} complex and also for a diiron^{III,III} compound.[11] The Mn(2)–O(4) butanol bond at 2.248 Å is in good agreement with the literature value of 2.22(6) Å.[12]

Each of the four benzimidazole N–H and the butanol O–H participate in hydrogen bonds to perchlorate anions in the lattice. The N···O(anion) distances range from 2.800 to 2.946 Å, and the O(4)···O(anion) distance is 2.931 Å. The waters in the lattice are only associated with the perchlorate anions.

IR Spectra. Comparison of the IR spectra of $[LMn_2^{II,II}X]Y_2$, μ-X = CH_3CO_2, $ClCH_2CO_2$; Y = ClO_4, BPh_4, CH_3CO_2, was used to determine the mode of acetate binding and to confirm homologous structures. All complexes have nearly identical absorption from ~600 to 350 cm^{-1} which serves to identify the dimanganese coordination mode seen in Figure 1. Minor differences can be shown to be from overlapping absorption by the counterions. The carboxylate band of $[LMn_2(CH_3CO_2)](ClO_4)_2$ occurs at 1674 cm^{-1} (antisymmetrical) and 1428 (symmetrical) which identifies a symmetrical bidentate μ-carboxylate. A table summarizing the key infrared bands may be found in the supplementary material.

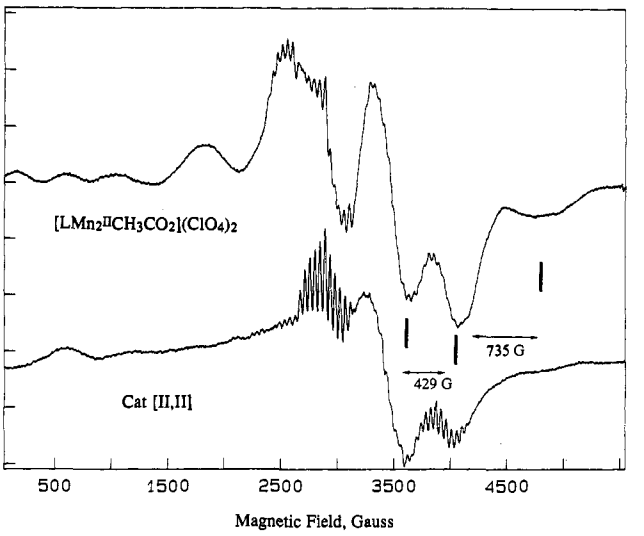

Figure 2. 9.34-GHz EPR spectra at $T \sim 60$ K of $MnCat^{II,II}$ (1 mg/ml) (bottom) and the synthetic analog (top) $[LMn_2(CH_3CO_2)](ClO_4)_2$ [1 mM, CH_2Cl_2/butanol].

EPR Spectra. Very similar EPR signals are observed for all of the μ-carboxylate bridged derivatives; data are presented only for $[LMn_2(CH_3CO_2)](ClO_4)_2$. Figure 2 compares the EPR spectra at 60 K of $MnCat^{II,II}$ from *T. thermophilus* vs. $[LMn_2(CH_3CO_2)](ClO_4)_2$ in butanol/CH_2Cl_2. Qualitative comparisons show that both spectra are centered at $g = 2.0$ and exhibit ^{55}Mn hyperfine and zero-field splittings typical of spin-coupled $Mn_2^{II,II}$ centers possessing an even spin electronic state origin.[6a] This includes an 11-line ^{55}Mn hyperfine structure with splitting equal to *ca.* 45 G and weak zero-field splittings with peak-to-peak separations as noted in Figure 2 of *ca.* 430 and 730 G.

Comparative studies of the temperature dependence of these EPR spectra reveal that both exhibit EPR-silent dimagnetic ground states at 2 K, in contrast to the halide derivative, $[LMn_2Cl_3]$ for which we reported an EPR-active ground state and weak ferromagnetic coupling.[6a] This ground-state signal and ferromagnetic coupling we now understand is incorrect, being due to a minor Mn^{2+} impurity which dominates at low temperature. The Mn^{2+} impurity occurs upon dissociation in butanol solvent. For the μ-carboxylate derivatives solubility in methanol and acetonitrile is much higher, and this problem is avoided. In this case, as the temperature is raised successive population of the first ($S = 1$) and second ($S = 2$) excited electronic states occurs, yielding the EPR signals in Figure 2. From the temperature dependence the relative state energies may be obtained (Heisenberg exchange interaction constant J), and from the dipolar part of the zero-field splitting the Mn–Mn distance may be obtained. A quantitative analysis is quite involved and will be presented elsewhere.[13a] Similar behavior is observed for $MnCat^{II,II}$, indicating a close correspondence with the electronic and spin properties of the catalase mimics. For example, for $MnCat^{II,II}$(phosphate) the Mn–Mn separation was found to be 3.59 vs. 3.54 Å for **1**, while $J = 5.6$ and 11.5 cm^{-1}, respectively.[13a]

Figure 3 compares the EPR spectra of the $Mn_2^{II,III}$ and $Mn_2^{III,IV}$ products of the oxidation of $[LMn_2(CH_3CO_2)](ClO_4)_2$ with $Pb(OAc)_4$, with two EPR signals observed upon oxidation of $MnCat^{II,II}$ isolated from *T. thermophilus*.[4a-d] The close spectral agreement supports the oxidation-state assignments originally

(10) (a) Suzuki, M.; Sugisawa, T.; Senda, H.; Oshio, H.; Uehara, A. *Chem. Lett.* **1989**, 1091–1094. (b) Chan, M. K.; Armstrong, W. H. *J. Am. Chem. Soc.* **1989**, *111*, 9121–9122. (c) Holman, T. R.; Andersen, K. A.; Anderson, O. P.; Hendrich, M. P.; Juarez-Garcia, C.; Munck, E.; Que, L., Jr. *Angew. Chem., Int. Ed. Engl.* **1990**, *29*, 921–923. (d) Uhlenbrock, S.; Krebs, B. *Angew. Chem., Int. Ed. Engl.* **1992**, *31*, 1647–1648.

(11) (a) Mikuriya, N.; Fujii, T.; Kawasaki, Y.; Tokii, T.; Oshio, H. *Chem. Lett.* **1990**, 1181–1184. (b) Tolman, W. B.; Bino, A.; Lippard, S. J. *J. Am. Chem. Soc.* **1989**, *111*, 8522–8523. (c) Tolman, W. B.; Liu, S.; Bentsen, J. G.; Lippard, S. J. *J. Am. Chem. Soc.* **1991**, *113*, 152–164.

(12) Orpen, A. G.; Brammer, L.; Allen, F. H.; Kennard, O.; Watson, D. C.; Taylor, R. J. *J. Chem. Soc., Dalton Trans.* **1989**, S1–S83.

(13) (a) Khangulov, S. V.; Pessiki, P. J.; Barynin, V. V.; Ash, D.; Dismukes, G. C. Structure and Energetics of the Triplet and Quintet Excited States of Dimanganese(II,II) Catalase, Liver Arginase and Dimanganese(II,II) Complexes. Manuscript submitted to *Biochemistry*. (b) Pessiki, P. J.; Dismukes, G. C. *J. Am. Chem. Soc.* following paper in this issue.

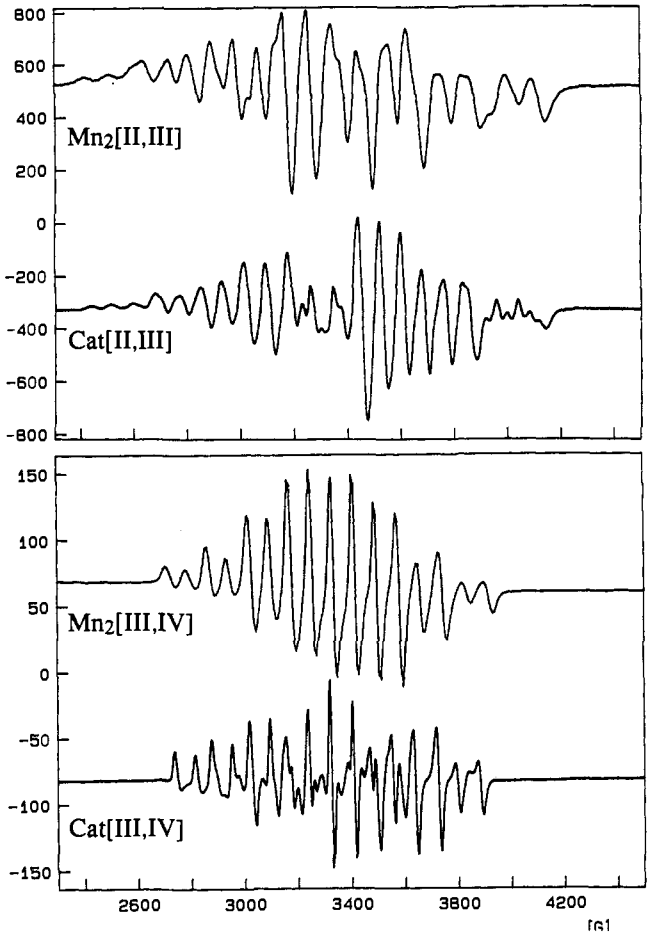

Figure 3. Comparison of the EPR spectra of the (II,III) and (III,IV) oxidation states of manganese catalase (Cat) and the oxidized forms of $[LMn_2(CH_3CO_2)](ClO_4)_2$. $Pb(OAc)_4$ was used to oxidize the synthetic analog. Conditions for the synthetic $Mn_2^{II,III}$: 50 mW, T = 10 K. Conditions for $Mn_2^{III,IV}$: power = 10 mW, T = 60 K.

suggested for the two MnCat signals. These are the first examples of these oxidation states formed in a functionally active catalase mimic, although as we shall demonstrate, these appear not to play a major role in catalase activity, a feature which is also true for the enzyme.[13b] In both $MnCat^{III,IV}$ and the $Mn_2^{III,IV}$ oxidation product, population of only the ground $S = {}^1/_2$ state is observed below 100 K, corresponding to strong antiferromagnetic coupling with a quartet–doublet energy gap of $\Delta E \geq 200$ cm^{-1}. The EPR signal for $Mn_2^{II,III}$ also corresponds to the ground $S = {}^1/_2$ electronic state. A partial temperature dependence study was performed from which we estimate ΔE(quartet–doublet) < 20 cm^{-1}.

Electrochemistry. Different electrochemical behavior is observed for the derivatives possessing a μ-carboxylate bridge vs a μ-Cl or μ-OH bridge, as illustrated by the cyclic voltammograms of $[LMn_2(CH_3CO_2)](ClO_4)_2$ and $[LMn_2Cl_3]$ in Figure 4 (lower and upper panels, respectively). The peak potentials and currents and the proposed assignments are given in Table 3. The initial oxidation of $[LMn_2(CH_3CO_2)](ClO_4)_2$ at 0.86 V is assigned to a two-electron process which is quasi-reversible. This is based on the following observations: the inequivalence of relative peak currents, $i^a_p/i^c_p \neq 1$, a doubling of the peak potential difference ($E_p^c - E_p^a$) with scan rate between 25 and 100 mv/s, and the independence of the ratio of (peak current)/(scan rate)$^{1/2}$, $i_p/v^{(1/2)}$, on scan rate (25–100 mv/s). This process is followed by a one-electron oxidation process at 1.30 V, which is paired with an irreversible reductive wave. The ratio of the peak heights for the first and second oxidation waves is 2. The μ-chloroacetate bridged derivative behaves similarly, except only the first oxidative

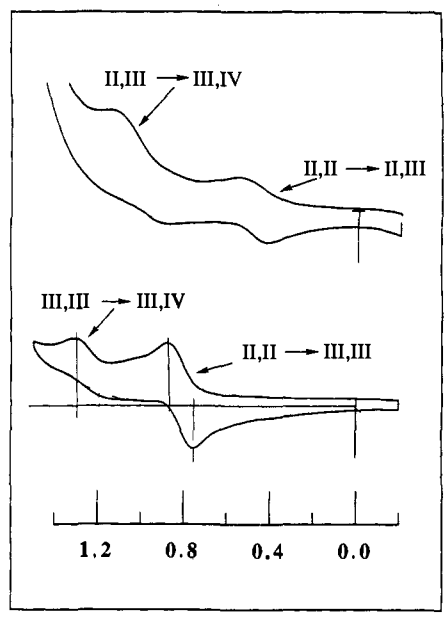

Figure 4. Cyclic voltammograms of $[LMn_2(CH_3CO_2)](ClO_4)_2$ and $[LMn_2Cl_3]$ demonstrating the effect of changing the bridging ligand from chloride to acetate. Conditions: Pt/Pt/SCE; solvent = acetonitrile; concn = 1 mM; scan rate = 100 mv/s; CR = 10 mA; supporting electrolyte = R_4NClO_4.

Table 3. Electrochemical Data for LMn_2XY_2[a]

XY_2	$E_{1/2}(1)$	$\Delta E_{pp}(1)$	$E_{ox}(2)$	$E_{red}(2)$	$E_{1/2}(2)$	$I(1)/I(2)$
$CH_3CO_2(ClO_4)_2$	0.81	0.11	1.30			2
$(ClCH_2CO_2)(ClO_4)_2$	0.86	0.24				NA
$ClCl_2$	0.49	0.13	1.13	0.89	1.01	0.5
$OH(Br)_2$	0.54	0.11	0.8			1

[a] Measurements were performed in acetonitrile using tetra-*n*-butylammonium perchlorate as the supporting electrolyte. A three electrode system was used in all measurements (Pt|Pt|SCE), and the scan rate was 100 mV/s. The last column, $I(1)/I(2)$ represents the oxidative peaks for the first and second waves.

wave is observed at 0.98 V within the limits of the solvent system. This behavior contrasts with that found previously for $[LMn_2(OH)Br_2]$ and $[LMn_2Cl_3]$.[6a] The latter exhibits a one-electron reversible oxidation process at 0.55 V, which is followed by a two-electron oxidation process, paired with an irreversible reductive wave. The ratio of the oxidative peak heights for the first and second processes is 0.5.

An EPR signal for a proposed $Mn_2^{II,III}$ species was obtained after partial electrochemical oxidation of $[LMn_2(CH_3CO_2)](ClO_4)_2$ at 0.85 V. This signal differs from the $Mn_2^{II,III}$ species obtained by chemical oxidation with $Pb(OAC)_4$. The two signals are compared in Figure 5 where one sees a 19-line spectrum which has an overall spectral breadth of 1884 G for the species obtained by electrochemical oxidation, while the oxidation product produced by $Pb(OAc)_4$ has 18 lines and an overall spectral breadth of 1734 G. This 150 G difference is largely attributable to a reduced ^{55}Mn hyperfine field in the latter species, as was established by spectral simulation.

Chemical Oxidation. The redox transformations were also examined by titration of $[LMn_2(CH_3CO_2)](ClO_4)_2$ with $Pb(OAc)_4$ in degassed acetonitrile solvent, using the distinct EPR spectra of the $Mn_2^{II,II}$, $Mn_2^{II,III}$, and $Mn_2^{III,IV}$ species to determine relative spin concentrations. The results are summarized in Table 4. As the titration progresses the $Mn_2^{II,II}$ oxidation state decreases until it is finally consumed between 2 and 4 equiv of $Pb(OAc)_4$ per Mn_2 complex. At 0.4 equiv of oxidant 43% of the original $Mn_2^{II,II}$ intensity is lost with no EPR signal appearing to replace it. The $Mn_2^{II,III}$ signal first appears between 0.4 and 1.0 equiv of oxidant, peaks near 2 equiv, and rapidly decreases above this. It is 28% of the maximum value at 4 equiv and is completely

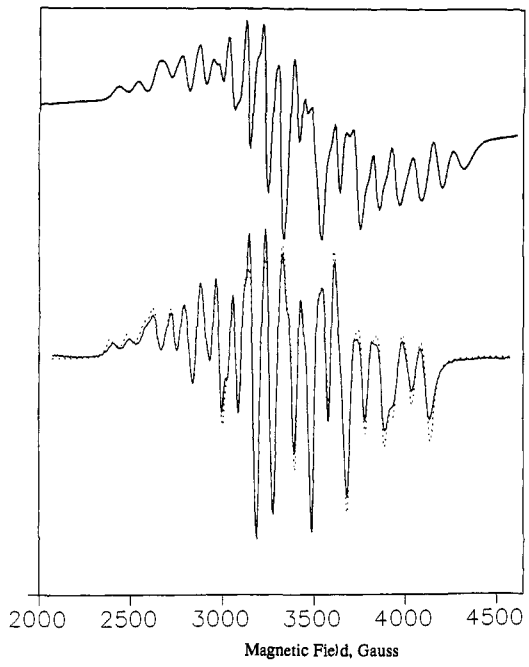

Figure 5. Comparison of the EPR signals of the $Mn_2^{II,III}$ oxidation state obtained by electrochemical oxidation in 1 M $(n\text{-}Bu)_4N(ClO_4)$ (top), and by $Pb(OAc)_4$ oxidation (bottom, solid). Concn = 1×10^{-3} M in CH_3CN, potential = 0.85 V. The dashed trace in the lower panel gives a simulation using the following parameters: ^{55}Mn: $|A_x|, |A_y|, |A_z|$ (MHz) = 534, 497, 716 (for Mn^{II}) and 271, 247, 275 (for Mn^{III}); g_x, g_y, g_z = 1.965, 1.977, 2.034; line width = 26 G; χ-squared R = .028.[15]

Table 4. Relative EPR Intensities of the Different Oxidation States during the Titration of 0.5 mmol of $[LMn_2CH_3CO_2](ClO_4)_2$ with $Pb(OAc)_4$

	concn of $Pb(CH_3CO_2)_4$, mmol				
EPR intensity	0.0	0.2	0.5	1.0	2.0
$Mn_2^{(II,II)}$	100	57	35	13	0
$Mn_2^{(II,III)}$	<5	<5	20	100	28
$Mn_2^{(III,IV)}$	<5	<5	<5	45	100

absent in excess oxidant. The concentration of the $Mn_2^{III,IV}$ species lags the $Mn_2^{II,III}$ species, growing in at higher concentrations of oxidant. It is the only EPR active species present in excess of oxidant.

Discussion

Structure. The ligand HL or its tetrakis(N-alkylated) derivative has been useful for synthesis of a number of multinuclear centers, including dinuclear copper(II) complexes[17] and di- and tetranuclear iron complexes[18] as well as dinuclear manganese complexes.[6a] Recently, $Mn_2^{II,II}$ complexes have been prepared by a number of different groups,[19] and other examples of multinuclear manganese[II] complexes which contain both five- and six-coordinate Mn ions have been reported.[20] The large size of the benzimidazolyl group and the facial geometry adopted by the three nitrogens of one arm of HL are important in restricting both the size of the metal cluster and the coordination number which can form. For examples, a related dimanganese complex in which the less bulky pyridyl group replaces the benzimidazoles gives six-coordinate Mn(II) ions.[10,21] Until recently only the meridonal isomers of the pyridyl based ligand were known which creates available coordination sites trans to the μ-alkoxo ligand. However, the facial geometry may also form under some conditions.[22]

We have tried unsuccessfully in the past to obtain large single crystals of the μ-chloride and bromide derivatives of LMn_2XY_2.[6a] This is also true for the BPh_4 derivatives described in this report. A probably explanation for this can be found in the lattice structure of $[LMn_2(CH_3CO_2)(n\text{-}BuOH)](ClO_4)_2 \cdot H_2O$. The amino hydrogens of all four benzimidazolyl groups are involved in hydrogen bonding with perchlorate anions in the lattice. Also, the water molecules in the lattice participate in hydrogen bonding donor with the perchlorate ions. Thus the counterions and solvent play critical roles in building the lattice.

The FAB mass spectrometry data and elemental analysis for $[LMn_2(CH_3CO_2)](ClO_4)_2$ as well as other derivatives, prior to recrystallization from butanol/CH_2Cl_2 did not reveal an alcohol ligand, as is observed in the X-ray structure after recrystallization. This indicates that the butanol is labile in solution. This is consistent with our earlier results showing that the bromide ions can be exchanged from $[LMn_2(OH)Br_2]$ in solution.[6a] Thus five-coordinate Mn(II) ions are favored for the μ-acetate derivatives in noncoordinating solvents.

The bridging acetate has an intense IR stretching band at 1564 cm^{-1} (antisymmetrical), and a weaker stretch at 1427 cm^{-1} (symmetrical). The difference, Δ = 137 cm^{-1}, is in the range expected for a symmetrically bridging acetate. For the μ-chloroacetate derivative the shift is 34 cm^{-1} toward higher energy which is in agreement with the literature.[23]

The X-ray structural data on the enzyme from *T. thermophilus* revealed a Mn–Mn separation of 3.6 ± 0.3 Å,[3] which compares with 3.54 Å for $[LMn_2(CH_3CO_2)](ClO_4)_2$. The Mn–Mn distance shortens to 2.7 Å in the $MnCat^{III,IV}$ enzyme obtained from *L. plantarum* which has been determined by EXAFS spectroscopy.[5c] This shortening has been interpreted to reflect formation of the $(\mu\text{-}O)_2$ linkage,[5c] a conclusion fully consistent with the strong magnetic coupling for this oxidation state.[4c,15] Formation of a μ-oxo bridge upon oxidation to the $Mn_2^{III,IV}$ state is a feature also observed for the catalase mimics.[24]

Redox Chemistry. As summarized in Table 3, a two-electron oxidation of $[LMn_2(RCHCO_2)](ClO_4)_2$ occurs at a Pt electrode at 0.81 V (R = H, quasi-reversible) or 0.86 V (R = Cl, quasi-reversible). In the presence of an excess of the $Mn_2^{II,II}$ species, this oxidation produces the EPR signal in Figure 5 (top) which we assign to a $Mn_2^{II,III}$ species produced by one-electron reduction. As summarized in Table 4 limited chemical oxidation with Pb-

(14) (a) Cooper, S. R.; Dismukes, G. C.; Klein, M. P.; Calvin, M. C. *J. Am. Chem. Soc.* **1978**, *100*, 7248–7252. (b) Dismukes, G. C.; Sheats, J. E.; Smegal, J. A. *J. Am. Chem. Soc.* **1987**, *109*, 7202–7204.

(15) (a) Zheng, M.; Dismukes, G. C. In *Research in Photosynthesis*; Proceedings of the 9th International Congress on Photosynthesis, Murata, N., Ed.; Kluwer Academic Publ.: Dordrecht, 1992; Vol. II, pp 305–308. (b) Zheng, M.; Khangulov, S. V.; Dismukes, G. C.; Barynin, V. V. *Inorg. Chem.*, in press.

(16) (a) Sheats, J. E.; Czernuziewicz, R.; Dismukes, G. C.; Rheingold, A.; Petrouleas, V.; Stubbe, J.; Armstrong, W. H.; Beer, R.; Lippard, S. J. *J. Am. Chem. Soc.* **1987**, *109*, 1435–1444. (b) Wieghardt, K.; Bossek, U.; Bonvoisin, J.; Beauvillain, P.; Girerd, J.-J.; Nuber, B.; Weiss, J.; Heinze, J. *Angew. Chem., Int. Ed. Engl.* **1986**, *25*, 1030–1034.

(17) McKee, V.; Zvagulis, M.; Dagdigian, J. V.; Patch, M. G.; Reed, C. A. *J. Am. Chem. Soc.* **1984**, *106*, 4765–4772.

(18) (a) Chen, Q.; Lynch, J. B.; Gomez-Romero, P.; Ben-Hussein, A.; Jameson, G. B.; O'Connor, C. J.; Que, L., Jr. *Inorg. Chem.* **1988**, *27*, 2673–2681. (b) Menage, S.; Brennan, B. A.; Juarez-Garcia, C.; Munck, E.; Que, L., Jr. *J. Am. Chem. Soc.* **1990**, *112*, 6423–6425. (c) Bremer, B.; Schepers, K.; Fleischhauer, P.; Haase, W.; Henkel, G.; Krebs, B. *J. Chem. Soc., Chem. Commun.* **1991**, 510–512.

(19) (a) Gultneh, Y.; Farooq, A.; Liu, S.; Karlin, K. D.; Zubieta, J. *Inorg. Chem.* **1992**, *31*, 3607–3611. (b) Yu, S.-B.; Lippard, S. J.; Shweky, I.; Bino, A. *Inorg. Chem.* **1992**, *31*, 3502–3504. (c) Flassbeck, C.; Wieghardt, K.; Bill, B.; Butzlaff, C.; Traughtwein, A. X.; Nuber, B.; Weiss, J. *Inorg. Chem.* **1992**, *31*, 21–26. (d) Kitajima, N.; Singh, U. P.; Amagai, H.; Masahisa, O. and Moro-oka, Y. *J. Amer. Chem. Soc.* **1991**, *113*, 7757–7758. (e) Yu, S.-B.; Wang, C.-P.; Day, E. P.; Holm, R. H. *Inorganic Chem.* **1991**, *30*, 4067–4074.

(20) (a) Mikuriya, N.; Fujii, T.; Kawasaki, Y.; Tokii, T.; Oshio, H. *Chem. Lett.* **1990**, 1181–1184. (b) Rardin, R. L.; Bino, A.; Poganiuch, P.; Tolman, W. B.; Liu, S.; Lippard, S. J. *Angew. Chem., Int. Ed. Engl.* **1990**, *29*, 812–814.

(21) (a) Suzuki, M.; Senda, H.; Suenaga, M.; Sugisawa, T.; Uehara, A. *Chem. Lett.* **1990**, 923–926. (b) Hagen, K. S.; Westmoreland, T. D.; Scott, M. J.; Armstrong, W. H. *J. Am. Chem. Soc.* **1989**, *111*, 1907–1908.

(22) Chan, M. K.; Armstrong, W. H. *J. Am. Chem. Soc.* **1991**, *113*, 5055–5057.

(23) Warrier, A. V. R.; Narayanan, P. S. *Spectrochimica Acta* **1967**, *234*, 1061–1067.

Scheme 1

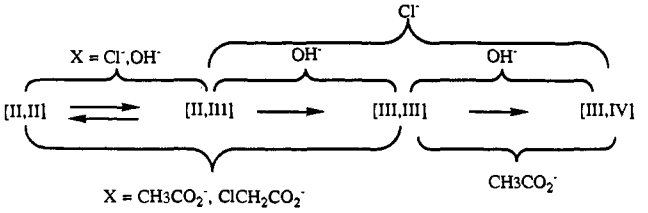

$(OAc)_4$ also yields an EPR-silent species, attributed to a $Mn_2^{III,III}$ species. As the titration progresses EPR signals for a $Mn_2^{II,III}$ species and finally a $Mn_2^{III,IV}$ species emerge. We can summarize both the electrochemical and chemical oxidation chemistry by eqs 2a–c. Oxidation of the $Mn_2^{II,II}$ starting material yields an EPR-silent $Mn_2^{III,III}$ species, which dismutates to yield two EPR-active mixed valence species, $Mn_2^{II,III}$ and $Mn_2^{III,IV}$, eqs 2a and 2b. The dismutation is not strongly favored, as seen by the quasi-reversible electrochemical behavior and also by the buildup of the $Mn_2^{III,III}$ species prior to formation of the $Mn_2^{II,III}$ species. An upper limit for the equilibrium constant for the dismutation reaction 2b is ≤0.1 M, based on the data in Table 4.

$$[II,II] \xrightarrow{Pb(CH_3CO_2)_4} [III,III] \quad (2a)$$

$$2[III,III] \rightleftarrows [II,III] + [III,IV] \quad (2b)$$

$$[III,IV] + [II,II] \rightleftarrows [II,III] + [III,III] \quad (2c)$$

$$2[II,II] \xrightarrow{Pb(CH_3CO_2)_4} 2[II,III] \quad (2d)$$

In the presence of excess $Mn_2^{II,II}$ species the $Mn_2^{III,IV}$ species formed by eq 2c is reduced to a $Mn_2^{II,III}$ species, accounting for the lag in the appearance of the $Mn_2^{III,IV}$ species in Table 4. Although the reaction proceeds as a two-electron oxidation, the net reaction appears as two one-electron oxidations, eq 2d.

The electrochemical behavior of the five-coordinate μ-acetate derivatives differs from the six-coordinate $[LMn_2Cl_3]$ and $[LMn_2(OH)Br_2]$ complexes, the latter of which exhibits three oxidations steps: A (II,III) (E_p = 0.60 V, reversible), B (III,III) (E_p = 0.80 V, irreversible), and C (III,IV) (E_p = 1.03 V, irreversible).[6a] The $[LMn_2Cl_3]$ complex exhibits only two resolved oxidations at E_p = 0.57 and 1.13 V, ascribed to processes A and B + C, respectively.[6a] This is summarized in Scheme 1. The resolution of the second oxidation process (B + C) into two thermodynamically resolved one-electron steps for $[LMn_2(OH)Br_2]$ was hypothesized to arise from proton ionization which lowers the potential from 1.13 (μ-Cl) to 0.80 V (μ-OH) in acetonitrile. For $[LMn_2(RCH_2CO_2)]^{2+}$ the reduction potential for the first oxidation process A increases by 0.31–0.37 V, creating an quasi-reversible two-electron process at 0.81–0.86 V attributed to processes (A + B). We attribute this substantial increase in the potential for the first oxidation to the lower coordination number of the Mn^{2+} ions in $[LMn_2(RCH_2CO_2)]^{2+}$ vs LMn_2Cl_3.

Comparing the μ-acetate and μ-chloroacetate derivatives, there is an increase in the midpoint potential by 0.05 V for the first oxidation process. Thus, chloroacetate stabilizes slightly the lower oxidation state of manganese. This is consistent with the anticipated weaker bonding by chloroacetate, as predicted on the basis of its lower pK_a versus acetic acid (ΔpK_a = 1.88).

The second oxidation process occurs at 1.30 V (irreversible) for the μ-acetate derivative which is +0.18 V above the μ-Cl derivative and +0.5 V above the μ-OH derivative. The μ-chloroacetate is undetected and presumed to fall above the allowed solvent range limited to 1.40 V. The lack of reversibility in the higher oxidation processes reflects additional chemistry which takes place once the $Mn_2^{III,IV}$ state is attained. Preliminary resonance Raman data suggests that this may involve formation of a μ-oxo bridge (Czernuszewicz, R. unpublished). The above results are summarized in Scheme 1.

Electrochemical data on MnCat are not available. However, the enzyme is known to spontaneously oxidize in air at alkaline pH to yield predominantly $MnCat^{III,IV}$.[4] The greatly increased thermochemical stability of the $Mn_2^{III,III}$ oxidation state in the enzyme vs the catalase mimics appears to be attributable to the difference in the ligand fields. The Mn ions in $MnCat^{III,IV}$ from *T. thermophilus* are coordinated predominantly to oxygen ligands comprised of $(\mu\text{-O})_2$ and polycarboxylato.[26] The greater anionic charge density in the enzyme vs the catalase mimics offers a reasonable explanation for the enhanced stability of the higher oxidation state.

EPR Spectra. Figure 3 demonstrates that there is close similarity between the EPR spectra of both $MnCat^{II,III}$ and $MnCat^{III,IV}$ vs the proposed $Mn_2^{II,III}$ and $Mn_2^{III,IV}$ products derived from oxidation with $Pb(OAc)_4$, respectively. As a class, EPR spectra of mixed valence dimanganese complexes have been extensively analyzed.[14,25] The EPR spectra of the catalase enzymes are the most highly resolved examples of these oxidation states and thus have provided the most detailed spectral simulations and insight.[5d,15] The spectral parameters derived from simulations of both oxidation states of the enzyme from *T. thermophilus* are known. From the spectral simulation of the $Mn_2^{II,III}$ oxidation product derived from $Pb(OAc)_4$, given as the dotted curve in Figure 5 (bottom), the hyperfine and g tensor parameters listed in the figure legend are obtained. This has revealed highly anisotropic ^{55}Mn hyperfine interactions to two inequivalent Mn ions with "trapped" valences in these frozen solutions. In both oxidation states the EPR signal originates from the lowest doublet electronic state. However, whereas the $Mn_2^{III,IV}$ spectrum and weak temperature dependence are consistent with a large doublet–quartet splitting ($|J| > 200\ cm^{-1}$), the large anisotropy of the $Mn_2^{II,III}$ spectrum and strong temperature dependence are known to be due to small doublet–quartet splitting relative to the zero-field splitting ($D/J < 1$).[15] The strong magnetic coupling in $Mn_2^{III,IV}$ implicates either $(\mu\text{-O})_2$ or $(\mu\text{-O})(\mu\text{-OR})$ bridging ligands.[7b,14] The Mn^{III} ions in both oxidation states of the enzyme and the models possess positive hyperfine anisotropy ($|A_z| > |A_x|, |A_y|$). This indicates that the ground state is well described as having the $(d_\pi)^3 d_{z^2}{}^1$ configuration, in which the sole antibonding d electron is located in a d_{z^2} orbital.[15] If the d_{z^2} orbital is located orthogonal to the plane defined by the rhombus $Mn_2(\mu\text{-O})(\mu\text{-OR})$, then the observed strong magnetic coupling can be understood.[7]

The core structure of the $Mn_2^{III,IV}$ product appears to be different from that observed in the $Mn_2^{II,II}$ oxidation state. We interpret the EPR signal of the $Mn_2^{III,IV}$ and it temperature dependence as evidence for a $Mn_2(\mu\text{-O})_2$ or $Mn_2(\mu\text{-O})(\mu\text{-alkoxo})$ core structure.[15] A different EPR pattern and temperature dependence can be expected in the absence of oxo bridges.[27]

(24) The complex $[LMn_2(\mu\text{-O})(OH)_2)](ClO_4)_2$ was synthesized as follows. HL (800 mg, 1.3 mmol) was suspended in 10 mL of acetone/methanol and 215 mg (0.88 mmol) of $Mn^{II}(OAc)_2{\cdot}4(H_2O)$ previously dissolved in a minimal amount of water was added with stirring. To this was added 20 mL of a one molar acetate buffer (pH = 4.5), and the pH of the solution was adjusted to 4.5. The mixture was cooled in an ice bath, and 60 mg (0.38 mmol) of solid $KMnO_4$ was added, upon which the reaction mixture darkens to a deep green color. After stirring for 1 h, 10 equiv of sodium perchlorate was added, and the reaction mixture was allowed to stand overnight. Filtration yields a green precipitate. Spectral data for $[LMn_2(\mu\text{-O})(OH)_2)](ClO_4)_3$: FT-IR (KBr, cm^{-1}) 631, 626 Mn–O–Mn; no infrared modes associated with an acetate were detected; FAB mass spectrometry $\{[LMn_2(\mu\text{-O})(OH^-)_2)](ClO_4^-)\}^{1+}$, (868 m/e); UV λ_{max} (CH_3CN) = 680 nm, ϵ = 110, $\Delta\nu_{1/2}$ = 58 nm. EPR spectroscopy demonstrates this species possesses an $S = {}^1/_2$ ground-state spin and a typical 16-line "multiline" signal.

(25) Diril, H.; Chang, H.-R.; Nilges, M. J.; Zhang, X.; Potenza, J. A.; Schugar, H.; J.; Isied, S. S.; Hendrickson, D. N. *J. Am. Chem. Soc.* **1989**, *111*, 5102–5114.

(26) Khangulov, S. V.; Sivaraja, M.; Barynin, V. V.; Dismukes, G. C. *Biochemistry* **1993**, *32*, 4912–4924.

(27) Larson, E.; Haddy, A.; Kirk, M. L.; Sands, R. H.; Hatfield, W. E.; Pecoraro, V. L. *J. Am. Chem. Soc.* **1992**, *114*, 6263–6265.

The EPR signal for the $Mn_2^{II,III}$ oxidation product exhibits a wider hyperfine field if oxidation of $[LMn_2(CH_3CO_2)](ClO_4)_2$ is done electrochemically in the presence of 1 M electrolyte, $(n\text{-butyl})_4N(ClO_4)$, as shown in Figure 5 (top). This new spectrum exhibits "19 lines" extending over 1884 G, which is wider by 150 G compared to both the $Mn_2^{II,III}$ species formed by $Pb(OAc)_4$ oxidation and the $MnCat^{II,III}$ spectrum. These spectral properties and the requirement for very low temperatures for detection indicate that it also belongs to the same oxidation class as $Mn_2^{II,III}$ complexes.[15,24] The structural origin of this increased ^{55}Mn hyperfine field is not clear, although presumably this reflects association between the $[LMn_2(CH_3CO_2)]^{2+}$ cations and the perchlorate anions of the electrolyte. It is possible that these form ion pairs in solution analogous to those observed in the crystal (Figure 1) or perhaps via weak coordination to the five-coordinate Mn ions, as occurs for the halides in both LMn_2Cl_3 and $LMn_2(OH)Br_2$. Unlike the strongly coupled $Mn_2^{III,IV}$ species, the weakly coupled $Mn_2^{II,III}$ species have EPR signals which are unusually sensitive to structural changes affecting the D/J ratio.[15] We propose that this arises from the weak coupling fostered by the (μ-OR)(μ-acetate) linkage and the possibility of exogenous ligand coordination to the five-coordinate Mn ions in $Mn_2^{II,III}$ species, in contrast to the (μ-O)(μ-OR) linkage and the six-coordinate Mn ions in the $Mn_2^{III,IV}$ oxidation state.

Acknowledgment. We thank Dr. V. Barynin for his interest and advice on manganese catalase, Mr. M. Zheng for an EPR simulation, and Prof. R. Czernuszewicz for preliminary resonance Raman experiments. This work was supported by the National Institutes of Health, GM39932. G.C.D. thanks the Princeton Chemistry Department for interim research support.

Supplementary Material Available: Infrared spectra (125–1700 cm^{-1}) for all derivatives (two figures) and X-ray structure report and data (eight tables) (19 pages). This material is contained in many libraries on microfiche, immediately follows this article in the microfilm version of the journal, and can be ordered from the ACS; see any current masthead page for ordering information.